Progress In Electromagnetics Research C, Vol. 54, 49–56, 2014

Simulation and Implementation of a New X-Band 1 : 4 Power Divider/Combiner Based on a New Waveguide *H*-Plane Folded Magic-T

Alaa A. Sarhan[1, *], Seyed H. Mohseni Armaki[1], Homayoon Oraizi[2], Nader Ghadimi[1], and Majid Tayarani[2]

Abstract—This paper presents the simulation and fabrication of a new power divider/combiner based on a new waveguide H-plane folded magic-T structure. Measurements of the fabricated magic-T confirm the accuracy of the optimization algorithms existing in the CST software (Genetic algorithm, Particle Swarm Optimization algorithm PSO etc.). The magic-T structure exhibits moderate bandwidth response in the frequency range of 8–10 GHz. Also, it shows that the return loss is better than −15 dB, the insertion loss about −3.4 dB, and the isolation between the two output ports better than −25 dB in the frequency range of 8.4–10 GHz, with good transmission phase characteristics. Based on this magic-T structure, a 1 : 4 power divider/combiner is simulated and tested. The measured results show that the insertion loss is about -6.5 ± 0.25 dB, the return loss less than −15 dB, the isolation among the output ports less than −25 dB, the combining efficiency about 89%, and the transmission phase differences are about ±2° in the frequency range of 8–10 GHz.

1. INTRODUCTION

Waveguides play an important role in RF systems. They can be found in a variety of devices such as power divider/combiner included in communication systems, radars, satellites, and medical equipments. In this paper, work is concentrated on 1 : 4 waveguide divider/combiner. Its key building block is the H-plane folded magic-T structure. It is first described in [1]. Various computational techniques have been used for the analysis of a waveguide magic-T structures. These techniques can be classified as: finite element/modal expansion [2], FDTD/Matrix-pencil method [3], and 3D boundary integral-resonant-mode expansion analysis of a magic-T structure employing a metal post and a matching septum [4]. Some optimization algorithms such as particle swarm optimization (PSO) [5] and genetical swarm optimization (GSO) [6] have been applied to enhance the frequency bandwidth. Nowadays, the presence of full-wave softwares, such as CST, HFSS, EMPro, FEKO, etc., will facilitate the analysis. In this work the CST software will be used for analysis, and we will also take benefit from the existing optimization algorithms in the CST software to obtain the desired results representing the perfect $[S]$ matrix of the magic-T structure. Using the CST software an H-plane folded magic-T structure is analyzed and optimized, then the simulated and measured results are compared. The novelty of this structure is the stepped septum used to improve the isolation without disturbing its symmetry. After that, based on this magic-T structure, three magic-T structure are used in a convenient topology to form a 1 : 4 power divider/combiner, which in its turn is simulated, fabricated, and measured. This type of divider/combiner falls in the category of circuit-level combiners [7, 8] and expresses a high power handling capability.

Received 10 September 2014, Accepted 29 September 2014, Scheduled 9 October 2014

* Corresponding author: Alaa Aldin Sarhan (alaaaldinn@gmail.com).

[1] Department of Electrical and Electronic Engineering, Malek Ashtar University of Technology, Tehran 15875-1774, Iran.

[2] Department of Electrical Engineering, Iran University of Science and Technology, Narmak, Tehran 16844, Iran.

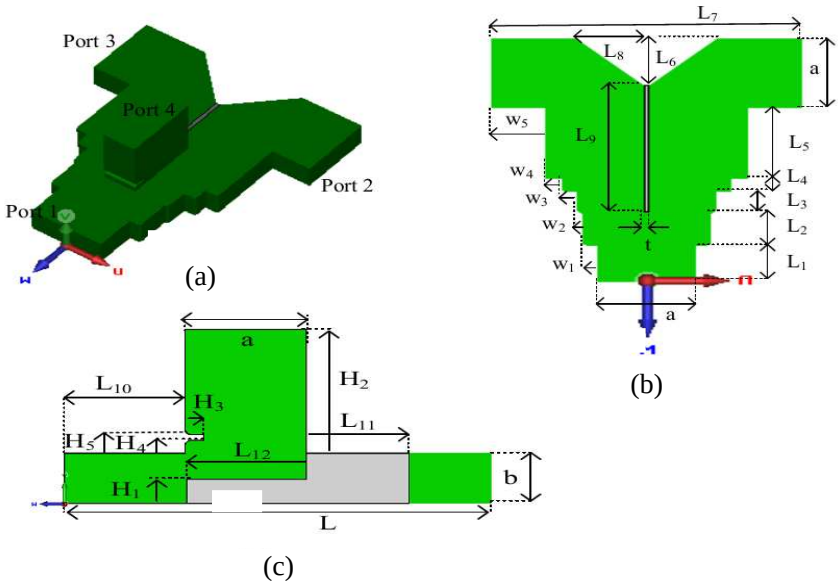

Figure 1. Topology of the waveguide H-plane folded magic-T structure (Green is vacuum and Grey is PEC. (The background material is PEC). (a) 3D view. (b) Bottom view. (c) Profile at the symmetrical plane V-W. (Direct Cartesian Coordinates UVW).

2. OPERATION PRINCIPLE OF THE H-PLANE FOLDED MAGIC-T

The waveguide H-plane folded magic-T structure, as well as many other waveguides structures, operates in the monomode region. The only propagating mode is the TE_{10}, and other modes are evanescent. Their amplitude diminishes as the distance from the waveguide discontinuity increases. Figure 1 illustrates the geometry under discussion and the labeling of the ports adopted in this article.

The perfect scattering matrix $[S]$ of this magic-T structure is summarized as follows

$$[S] = \frac{1}{\sqrt{2}} \begin{bmatrix} 0 & 1 & 1 & 0 \\ 1 & 0 & 0 & 1 \\ 1 & 0 & 0 & -1 \\ 0 & 1 & -1 & 0 \end{bmatrix} \tag{1}$$

Equation (1) indicates that when signal is injected into the H-port (port 1), the output signal is divided equally between ports 2 and 3, and they are in phase. Also, it shows that when signal is injected into E-port (port 4), the output signal is equally divided between ports 2 and 3, but this time they are out of phase (180 degrees out of phase).

The isolation between ports 1 and 4 comes simply by the properties of E- and H-plane T-junctions. However, the isolation between ports 2 and 3 is achieved by using the stepped PEC septum inserted in the V-W plane and also by the PEC septum inserted into the port 4 arm (see Figure 1). All of this is done without disturbing the symmetry of the structure. The four ports are fully matched by using, in addition to the two septums mentioned above, the stepped matching sections in the port 1 arm.

3. SIMULATION AND EXPERIMENTAL RESULTS OF THE PROPOSED MAGIC-T

In this section, two things will be investigated. First, the power-handling capacity of the optimized air-filled magic-T structure and second its $[S]$ matrix parameters.

3.1. Power-Handling Capacity of the Proposed Magic-T

In an air-filled rectangular waveguide, the electric field of the TE_{10} varies as $E_y = E_{10}\sin(\pi x/a)$. Its maximum value occurs in the middle of the guide ($x = a/2$). The power-handling capacity of an air-

filled transmission line or waveguide is usually limited by voltage breakdown, which occurs at a field strength of about $E_d = 3\,\mathrm{MV/m}$ for room temperature air at sea level pressure.

For TE_{10} mode, the power transferred inside the rectangular waveguides [9] is

$$P_{\mathrm{TE}_{10}} = \frac{abE_{10}^2}{480\pi}\sqrt{1-\left(\frac{\lambda}{2a}\right)^2} \tag{2}$$

Here, a and b denote the width and height of the waveguide, respectively.

Thus the maximum power capacity before breakdown is

$$P_{\text{max-TE}_{10}} = \frac{abE_d^2}{480\pi}\sqrt{1-\left(\frac{\lambda_{\min}}{2a}\right)^2} \tag{3}$$

At 10 GHz the maximum peak power capacity of a standard WR90 rectangular waveguide operating in the TE_{10} mode is about 2300 kW. In addition, it is good engineering practice to provide a safety factor at least two, so the maximum powers that can be safely transmitted should be limited to about half of the above value. Now, if we come back to the optimized waveguide H-plane folded magic-T, for which its optimized dimensions are shown in Table 1, the distribution of the 3D absolute maximum E-field distribution inside the structure in the symmetrical plane V-W at the frequency 10 GHz can be obtained by using CST software as shown in Figure 2.

Referring to Figure 2, the maximum value of the E-field can be found to be 10994 V/m. We have $H_1 = 4.9\,\mathrm{mm}$. If we measure the $|E_y|$ along a line at $H_1 = 4.95\,\mathrm{mm}$ in the V-W symmetrical plane, this line starts at port 1 and ends in the PEC septum. The result of this measurement using the CST software is shown in Figure 3.

From Figure 3 it is easy to note that the ratio of the maximum E-field (about 10410 V/m) to the field near port 1 (about 2000 V/m) is about 5.2. From this ratio and by using Equation (3), we can say that this magic-T structure can handle a maximum power about 85.06 kW before breakdown.

Table 1. Optimized dimensions (mm) of the H-plane folded magic-T structure.

L_1	L_2	L_3	L_4	L_5	L_6	L_7	L_8	L_9	L_{10}	L_{11}	L_{12}	L
12.2	**10.7**	**6.9**	**4.4**	**23.8**	**15.6**	**71.4**	**15.6**	**42.1**	**22.9**	**19.5**	**22.6**	**80.9**
W_1	W_2	W_3	W_4	W_5	H_1	H_2	H_3	H_4	H_5	a	b	t
3.35	**1.1**	**3.6**	**4**	**12.2**	**4.9**	**25**	**3.5**	**2.6**	**3.8**	**22.9**	**10.2**	**1.2**

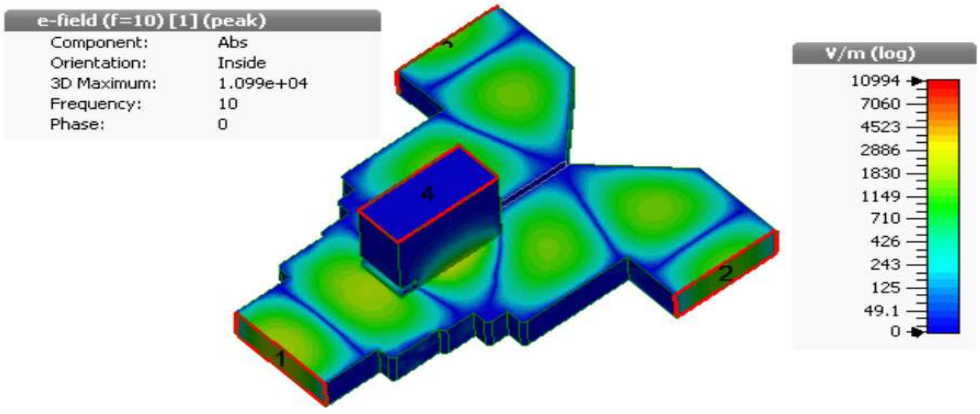

Figure 2. Absolute maximum 3D E-field distribution at frequency 10 GHz.

3.2. Comparing the Simulated and Measured [*S*] Matrix Parameters

Figure 4 shows the fabricated waveguide H-plane folded magic-T structure. The vector network analyzer (VNA) HP8510 is used for measurement. The simulated and measured transmission $[S]$ parameters are shown in Figure 5. It is shown that the measured insertion loss is about -3.4 dB in the frequency range of 8–10 GHz including the adaptors losses which is about -0.2 dB in average. The little difference between the two measured transmission losses is due to assembly deficiencies.

The simulated and measured reflection $[S]$ parameters are shown in Figure 6. It is shown that the measured return losses are all less than -15 dB in the frequency range of 8–10 GHz. The differences between the simulated and measured parameters are due to assembly deficiencies and especially in the waveguide port flanges.

Figure 7 shows the simulated and measured isolation $[S]$ parameters. The differences between simulated and measured results are due to the imperfections in the used matching loads (here adapters from waveguide to SMA 50 Ohm connectors and SMA 50 Ohm matching loads are used).

Figure 8 shows the measured transmission $[S]$ parameter phases and indicates that the results are in accordance with the ideal $[S]$ matrix explained in Equation (1).

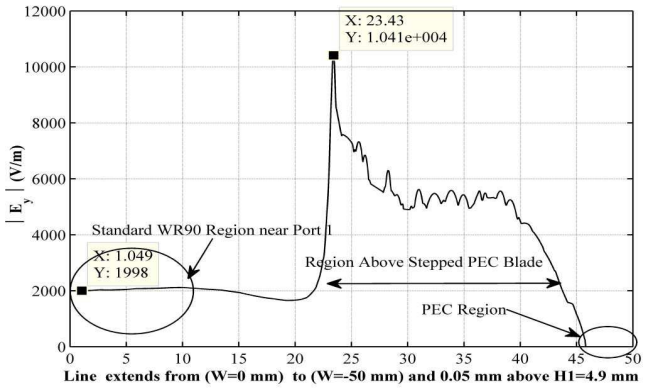

Figure 3. Magnitude of E_y at $f = 10$ GHz along a line extends from point ($U = 0$, $V = 4.95$ mm, $W = 0$) to point ($U = 0$, $V = 4.95$ mm, $W = -50$ mm) (see Figure 1).

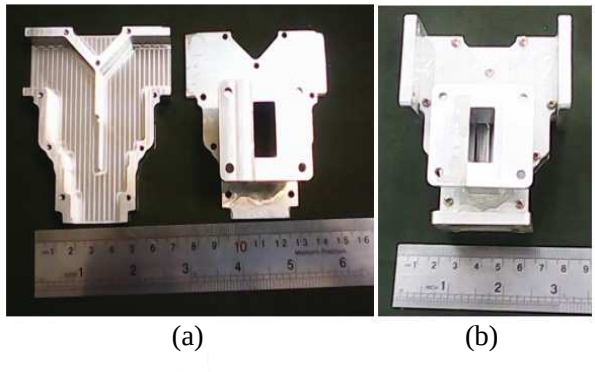

Figure 4. The fabricated waveguide H-plane folded magic-T structure. (a) Inside view with cover. (b) Complete assembled view.

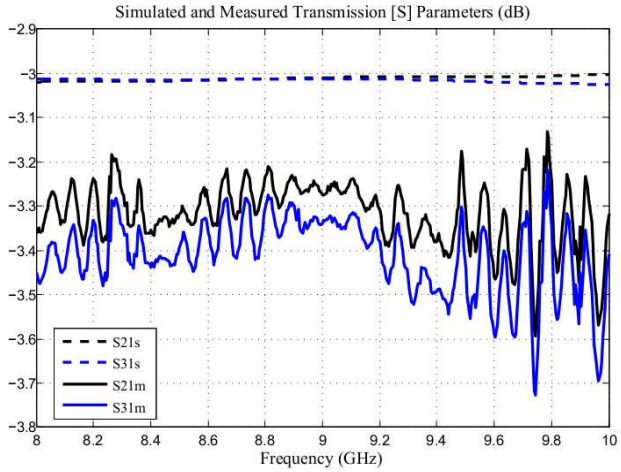

Figure 5. The simulated and measured transmission $[S]$ parameters (s, m indices mean simulated and measured respectively).

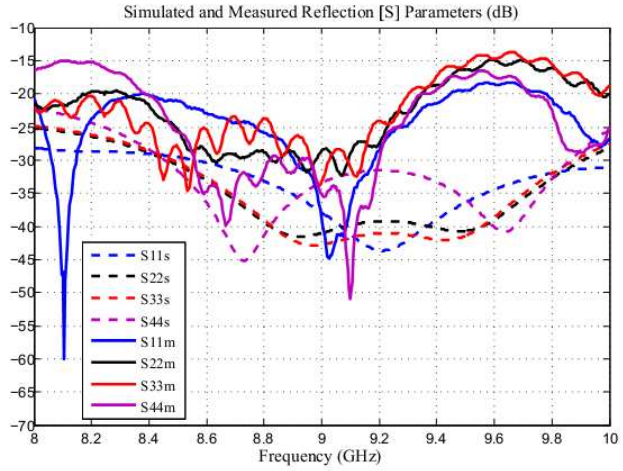

Figure 6. The simulated and measured reflection $[S]$ parameters (s, m indices mean simulated and measured respectively).

4. SIMULATION AND EXPERIMENTAL RESULTS OF THE PROPOSED DIVIDER/COMBINER

Figure 9 shows the 3D absolute maximum E-field distribution inside the structure of the proposed $1:4$ combiner/divider and the labeling of the ports adopted in this article. This structure consists basically of three magic-T structures proposed before. Port 1 is a waveguide input port in the divider structure, or it is the output port in the combiner structure. Ports 2, 3, 4, and 5 are the output ports in the divider structure or the input ports in the combiner structure. These ports are 50 Ohm SMA Connectors (like adapter from coaxial to waveguide). The rest of ports are waveguide ports.

Figure 10 shows the fabricated $1:4$ power divider/combiner based on waveguide H-plane folded magic-T structure simulated and measured before. The simulated and measured transmission $[S]$ parameters are shown in Figure 11, which shows that the transmission $[S]$ parameters are about -6.5 ± 0.25 dB in the frequency range of 8–10 GHz. This value includes the losses of the commercial connectors and the adaptor (waveguide to SMA connector) used for port 1. The little differences are due to both the imperfections in fabrication and assembly of the structure.

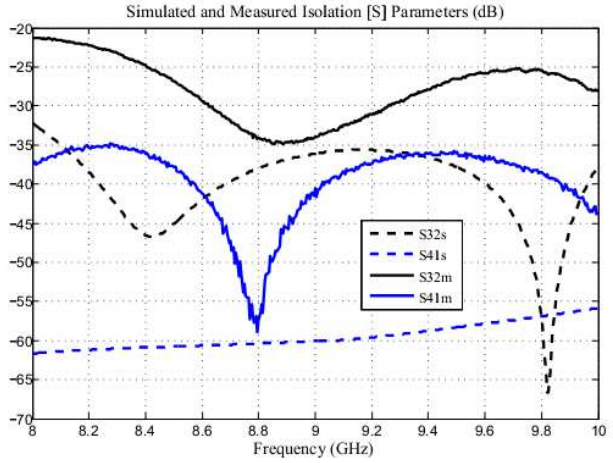

Figure 7. The simulated and measured isolation $[S]$ parameters (s, m indices mean simulated and measured respectively).

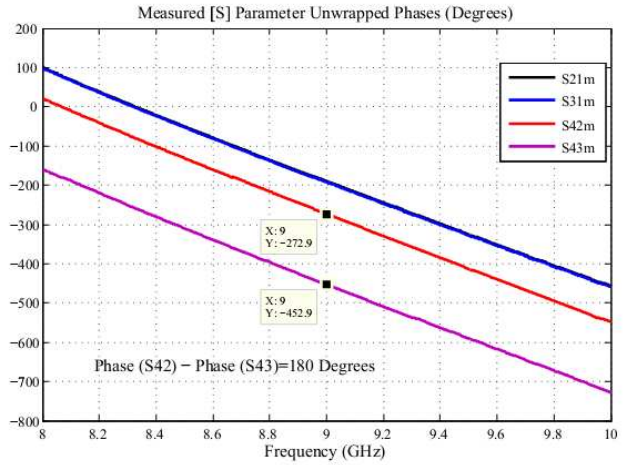

Figure 8. The measured transmission $[S]$ parameter phases (m index means measured).

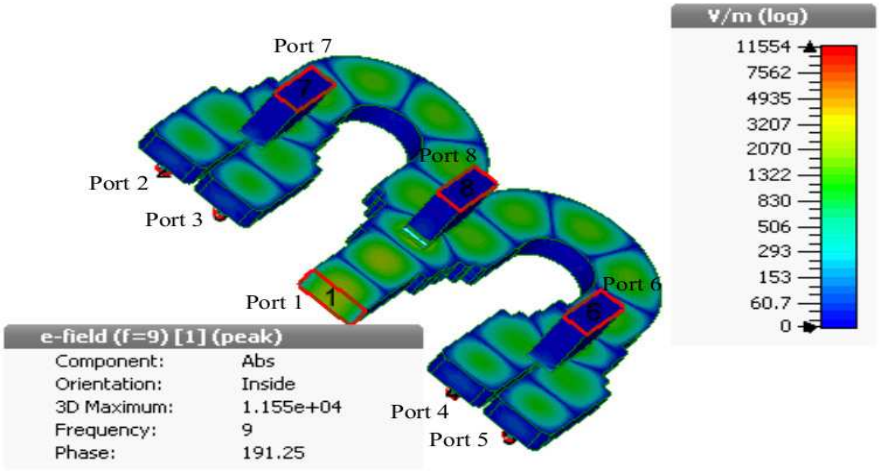

Figure 9. Absolute maximum 3D E-field distribution for the divider/combiner based on the above proposed magic-T structure at the frequency 9 GHz.

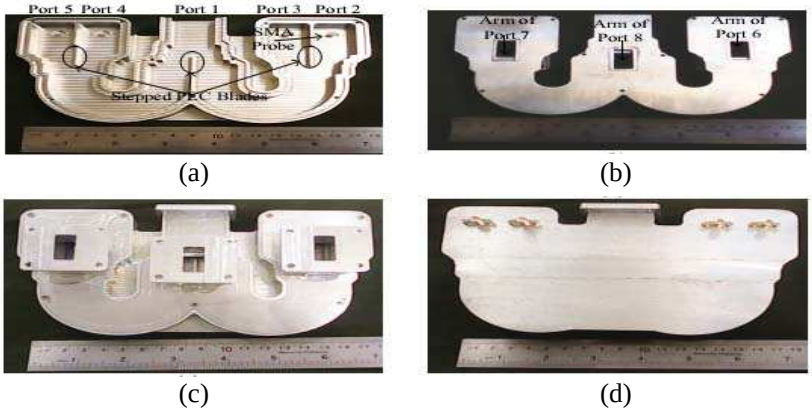

Figure 10. The fabricated divider/combiner based on the waveguide H-plane folded magic-T structure. (a) Inside view of the divider/combiner. (b) Cover with the three E-plane arms. (c) Top view of the assembled divider/combiner. (d) Bottom view of the assembled divider/combiner.

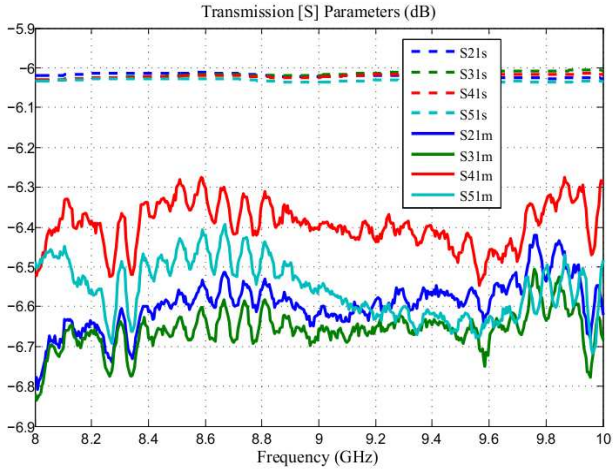

Figure 11. The simulated and measured transmission $[S]$ parameters (s, m indices mean simulated and measured respectively).

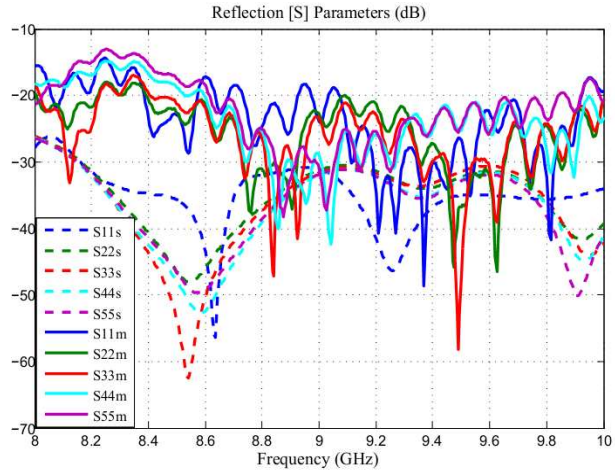

Figure 12. The simulated and measured reflection $[S]$ parameters (s, m indices mean simulated and measured respectively).

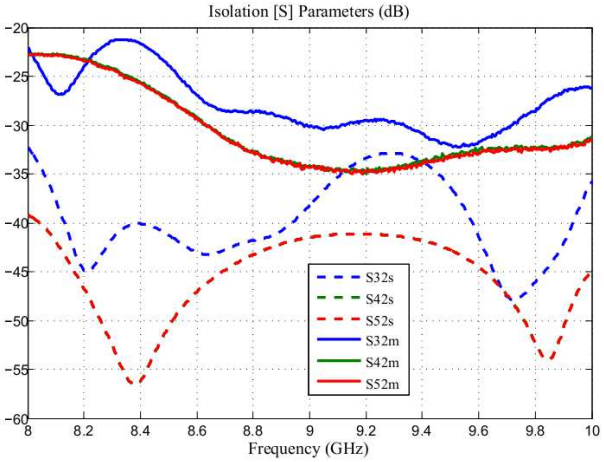

Figure 13. The simulated and measured isolation $[S]$ parameters (s, m indices mean simulated and measured respectively).

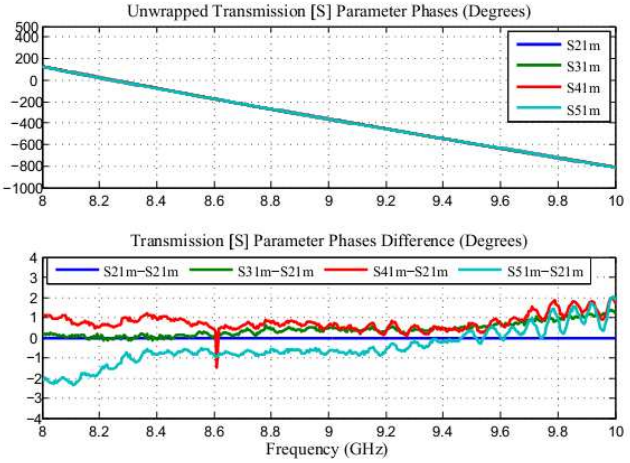

Figure 14. The measured transmission $[S]$ parameter phases and their differences relative to phase ($S_{21}m$). (m index means measured).

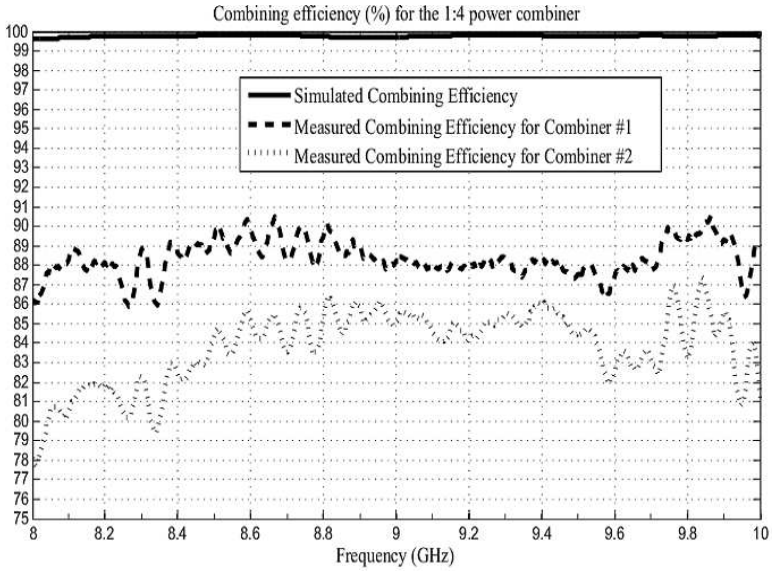

Figure 15. The simulated and measured combining efficiency for both 1 : 4 combiners #1 and #2.

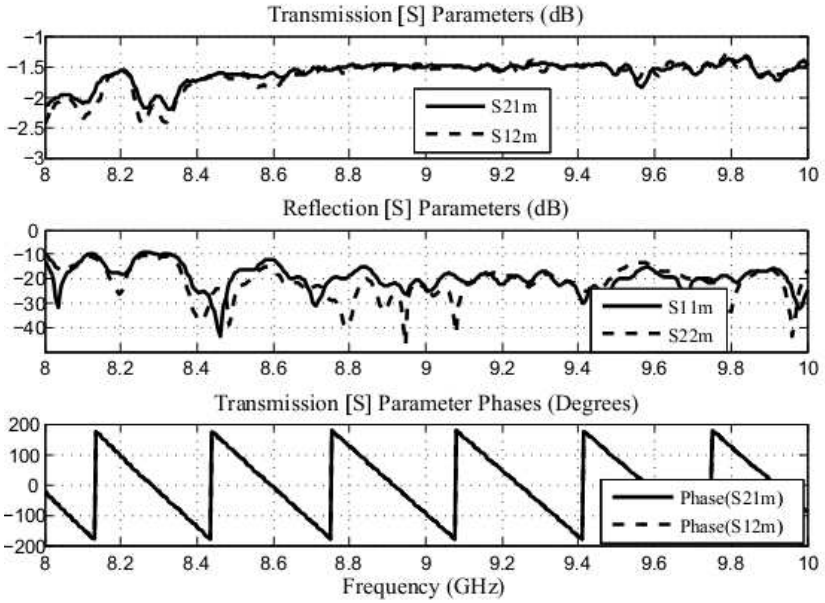

Figure 16. The measured $[S]$ parameters for the back-to-back 1 : 4 divider/combiner. (m index means measured).

The simulated and measured reflection $[S]$ parameters are shown in Figure 12, which shows that the measured return losses are all less than -15 dB in average in the frequency range of 8–10 GHz. The differences between the simulated and measured parameters are due to assembly and fabrication deficiencies and especially in the waveguide port 1 flange for S_{11}.

Figure 13 shows the simulated and measured isolation $[S]$ parameters and indicates a good isolation among output ports relative to port 2. The differences between the simulated and measured results are due to imperfections of the used matching loads and also to the deficiencies in the divider/combiner mechanical assembly.

Figure 14 shows the measured transmission phases and indicates that the differences in the

transmission phases relative to the phase of S_{21} are about $\pm 2^\circ$ in the frequency range of 8–10 GHz.

Figure 15 shows the simulated and measured combining efficiency for both 1 : 4 combiners #1 and #2. This calculation is done by using the commercial software ADS from Agilent. It is easy to note that combiner #1 is better for the combining stage and combiner #2 better for the dividing stage. The difference in combining efficiency of the two combiners is due to deficiencies in fabrication and assemblage.

The last test in this article is back-to-back divider/combiner $[S]$ parameters measurement. For this purpose, a second 1 : 4 divider/combiner from the same kind is fabricated and tested. The four cables used to connect the two structures have an insertion loss about -0.2 dB and return loss less than -20 dB in average, and also they have the same length. The results for this measurement are shown in Figure 16.

These results show that these cables can be replaced safely by MMIC high power solid state power amplifiers. This can be done because of the good characteristics introduced in this article for this type of dividers/combiners.

5. CONCLUSION

Both the waveguide H-plane folded magic-T structure and the power divider/combiner based on this magic-T structure have been simulated, optimized using the CST software, and measured. The measured results have shown agreement with the simulated ones. A good return loss, insertion loss, and isolation are achieved in the frequency range of 8–10 GHz. The power divider/combiner also demonstrates low dispersion. Good isolation and high power handling capacity can be achieved by the novel structure. Also, a combining efficiency of about 89% in average is obtained in the same frequency range.

ACKNOWLEDGMENT

The authors express their gratitude to Mrs. Hamid Dost and Khosro Shahristani for their help in the mechanical assembly.

REFERENCES

1. Tyrell, W., "Hybrid circuits for microwaves," *Proceedings of the IRE*, Vol. 35, No. 11, 1294–1306, 1947.
2. Shen, Z., C. L. Law, and C. Qian, "Hybrid finite-element-modal-expansion method for matched magic T-junction," *IEEE Trans. Magn.*, Vol. 38, No. 2, 385–388, Mar. 2002.
3. Ritter, J. and F. Arndt, "Efficient FDTD/matrix-pencil method for the full-wave scattering parameter analysis of waveguiding structures," *IEEE Trans. Microw. Theory Tech.*, Vol. 44, No. 12, 2450–2456, Dec. 1996.
4. San Blas, A. A., F. Mira, V. E. Boria, B. Gimeno, M. Bressan, and P. Arcioni, "On the fast and rigorous analysis of compensated waveguide junctions using off-centered partial-height metallic posts," *IEEE Trans. Microw. Theory Tech.*, Vol. 55, No. 1, 168–175, Jan. 2007.
5. Robinson, J. and Y. Rahmat-Samii, "Particle swarm optimization in electromagnetic," *IEEE Trans. Antennas Propag.*, Vol. 52, No. 2, 397–407, Feb. 2004.
6. Hwang, K. C., "Design and optimization of a broadband waveguide magic-T using a stepped conducting cone," *IEEE Microwave and Wireless Components Letters*, Vol. 19, No. 9, 539–541, Sep. 2009.
7. Russell, K. J., "Microwave power combining techniques," *IEEE Trans. Microw. Theory Tech.*, Vol. 27, No. 5, 472–478, May 1979.
8. Chang, K. and C. Sun, "Millimeter-wave power-combining techniques," *IEEE Trans. Microw. Theory Tech.*, Vol. 31, No. 2, 91–107, Feb. 1983.
9. Wu, H. C. and W. B. Dou, "A rigorous analysis and experimental researches of waveguide magic Tee at W-band," *Progress In Electromagnetics Research*, Vol. 60, 131–142, 2006.